ETH
Eidgenössische Technische Hochschule Zürich
Swiss Federal Institute of Technology Zurich

Seminar for Applied Mathematics SAM

Dispersion Analysis of Plane Wave Discontinuous Galerkin Methods

C. Gittelson and R. Hiptmair

Research Report No. 2012-42

Seminar für Angewandte Mathematik
Eidgenössische Technische Hochschule
CH-8092 Zürich
Switzerland

- Submitted to International Journal for Numerical Methods in Engineering (IJNME)

DISPERSION ANALYSIS OF PLANE WAVE DISCONTINUOUS GALERKIN METHODS

Claude J. Gittelson[1] and Ralf Hiptmair[2]

Abstract. The plane wave discontinuous Galerkin (PWDG) method for the Helmholtz equation was introduced and analyzed in [Gittelson, C., Hiptmair, R., and Perugia, I. Plane wave discontinuous Galerkin methods: Analysis of the h-version. *Math. Model. Numer. Anal. 43* (2009), 297–331] as a generalization of the so-called ultra-weak variational formulation, see [O. Cessenat and B. Després, *Application of an ultra weak variational formulation of elliptic PDEs to the two-dimensional Helmholtz equation*, SIAM J. Numer. Anal., 35 (1998), pp. 255–299]. The method relies on Trefftz-type local trial spaces spanned by plane waves of different directions, and links cells of the mesh through numerical fluxes in the spirit of discontinuous Galerkin methods.

We conduct a partly empirical dispersion analysis of the method in a discrete translation invariant setting by studying the mismatch of wave numbers of discrete and continuous plane waves travelling in the same direction. We find agreement of the wave numbers for directions represented in the local trial spaces. For other directions the PWDG methods turn out to incur both phase and amplitude errors. This manifests itself as a *pollution effect* haunting the h-version of the method. Our dispersion analysis allows a quantitative prediction of the strength of this effect and its dependence on the wave number and number of plane waves.

2010 Mathematics Subject Classification. 65N30,78M30.

Version: December 20, 2012

1. Introduction

We consider the homogeneous Helmholtz equation

$$-\Delta u - \omega^2 u = 0\,, \tag{1}$$

on d-dimensional space as our model partial differential equation governing the isotropic propagation of scalar waves. Here $\omega > 0$ denotes the wave number related to the wavelength λ by $\lambda = \frac{2\pi}{\omega}$.

Local mesh-based discretizations of (1) are haunted by the so-called pollution effect [6], which refers to the accumulation of amplitude and phase error due to numerical dispersion. The former describes the undesirable damping of "discrete plane waves", the latter the deviation of their wave numbers from the exact value ω, cf. [6, 9].

Keywords and phrases: Helmholtz equation, plane wave, discontinuous Galerkin, numerical dispersion

[1] Department of Mathematics, Purdue University, West Lafayette, IN 47907, USA

[2] Seminar for Applied Mathematics, ETH Zurich, 8092 Zürich, Switzerland

The classical approach to investigating numerical dispersion considers the discretization scheme for the unbounded domain $\mathbb{R}^d$ on infinite meshes that are invariant under a discrete group of translations. Then discrete Bloch waves can be found by solving small non-linear eigenvalue problems, see, among others, the articles [9, 16, 17]. Fully symbolic computations become possible when the scheme is intrinsically of tensor product type, see the work of M. Ainsworth [1, 3–5]. In more general settings, quantitative information about numerical dispersion can solely be obtained from numerical computations.

An idea meant to curb the pollution effect is to incorporate information on the wave number ω into finite dimensional trial spaces and use those for a Galerkin-type discretization of (1). One such attempt is the so-called plane wave discontinuous Galerkin (PWDG) methods introduced in [10] and further analyzed in [11–13]. These generalize the ultra-weak variational formulation (UWVF) scheme of Cessenat and Despres [7, 8, 14, 15], which has attracted considerable attention.

Numerical experiments in [10, Section 5] clearly conveyed that the h-version of PWDG that seeks to enhance accuracy through refining the mesh is afflicted by the pollution effect. This article pursues a quantitative analysis of this effect by studying the strength of numerical dispersion present in several variants of PWDG among them UWVF. We pursue this for both triangular and quadrilateral meshes in 2D. For want of tensor product structure we have to rely on numerical approximation in the final step. However, this gives information of almost the same quality as closed form expressions.

In the next section we introduce PWDG to the extent needed for dispersion analysis. Then we briefly review the setting and gist of dispersion analysis in Section 3. Numerical computations that yield comprehensive quantitative information about the dispersive nature of the PWDG-discretized Helmholtz equation on selected grids in two dimensions are documented in Section 5. Section 4 discusses details of the computational methodology.

The results of our numerical dispersion analysis for PWDG can be summarized as follows:

- All variants of PWDG under investigation are affected by numerical dispersion, which will inevitably engender a pollution effect for the h-version. Different choices of PWDG flux coefficients seem to have only a minor impact.
- Relative dispersion in 2D grows like $O(\omega^{2q})$, $q := \lfloor \frac{p-1}{2} \rfloor$, where p is the fixed number of equispaced plane waves per cell.
- Relative dispersion enjoys an exponential decrease in p.
- An increase in the number of degrees of freedom buys a greater reduction in numerical dispersion for PWDG than for standard Lagrangian finite elements.

2. Plane Wave Discontinuous Galerkin Methods (PWDG)

From [10, Sect. 2] we briefly recall the definition of the PWDG discretization of the Helmholtz equation (1). Since dispersion analysis ignores boundaries, we only consider the unbounded domain $\Omega = \mathbb{R}^d$, $d = 2, 3$. To begin with, we equip Ω with an infinite triangulation $\mathcal{T}_h = \{K\}$ with polyhedral cells K of equal size, and write $\mathcal{F}_h$ for its skeleton, that is, the union of edges ($d = 2$) or faces ($d = 3$).

Secondly, as a linear Galerkin method, PWDG involves a sesquilinear form whose definition relies on the triangulation $\mathcal{T}_h$. As explained in [10, Sect. 2], by means of local integration by parts and suitably defined numerical fluxes we arrive at the following PWDG sesquilinear form

$$b_h(u, v) := a_h(u, v) - \omega^2 (u, v)_{\mathbb{R}^d} ,$$

with $(\cdot, \cdot)_{\mathbb{R}^d}$ the $L^2(\mathbb{R}^d)$ inner product and

$$\begin{aligned} a_h(u, v) := & \sum_{K \in \mathcal{T}_h} \int_K \nabla u \cdot \nabla \overline{v} \, \mathrm{d}\boldsymbol{x} - \int_{\mathcal{F}_h} [\![u]\!]_N \cdot \{\!\{\overline{\nabla_h v}\}\!\} \, \mathrm{d}S - \int_{\mathcal{F}_h} \{\!\{\nabla_h u\}\!\} \cdot [\![\overline{v}]\!]_N \, \mathrm{d}S \\ & - \frac{\beta}{\mathrm{i}\omega} \int_{\mathcal{F}_h} [\![\nabla_h u]\!]_N [\![\overline{\nabla_h v}]\!]_N \, \mathrm{d}S + \mathrm{i}\omega\alpha \int_{\mathcal{F}_h} [\![u]\!]_N \cdot [\![\overline{v}]\!]_N \, \mathrm{d}S , \end{aligned} \tag{2}$$

see [10, Eq. (4.3)]. The positive parameters $\alpha, \beta > 0$ reflect the choice of numerical fluxes, and ∇_h stands for a piecewise gradient on $\mathcal{T}_h$. We have also used the standard notations for

$$\begin{aligned} \text{averages:} \quad & \{\!\{\nabla_h v\}\!\} := \tfrac{1}{2}(\nabla v_{|K^+} + \nabla v_{|K^-}) \,, \\ \text{jumps:} \quad & [\![u]\!]_N := u_{|K^+}\, \boldsymbol{n}^+ + u_{|K^-}\, \boldsymbol{n}^- \,, \end{aligned}$$

across an edge/faces separating two cells K^+ and K^-. It goes without saying that sufficient regularity is required for the argument functions of a_h. Piecewise smooth functions with respect to $\mathcal{T}_h$ are admissible, of course. As will be elucidated in Section 3, dispersion analysis can dispense with knowledge of a "right hand side" source functional.

The third ingredient of a PWDG method are trial and test spaces $V_h \subset V$ spanned by plane waves locally. In detail, let the plane wave space $PW_\omega(\mathbb{R}^d)$ be characterized by the number $p \in \mathbb{N}$ of plane waves and p mutually different directions $\boldsymbol{d}_j$, $j = 1, \dots, p$:

$$PW_\omega(\mathbb{R}^d) := \{v \in C^\infty(\mathbb{R}^d) : \; v(\boldsymbol{x}) = \sum_{j=1}^{p} \gamma_j \exp(\mathrm{i}\omega \boldsymbol{d}_j \cdot \boldsymbol{x}), \; \gamma_j \in \mathbb{C}\} \,. \tag{3}$$

In particular, in all numerical computations (for $d = 2$) we will use evenly spaced directions

$$\boldsymbol{d}_j = \begin{pmatrix} \cos(\frac{2\pi}{p}(j-1) + \psi) \\ \sin(\frac{2\pi}{p}(j-1) + \psi) \end{pmatrix} \,, \quad j = 1, \dots, p \,, \quad \psi \in \mathbb{R} \text{ fixed} \,. \tag{4}$$

Now we are in a position to define the global trial and test spaces for PWDG

$$V_h := \{v \in L^2_{\mathrm{loc}}(\mathbb{R}^d) : \; v_{|K} \in PW_\omega(\mathbb{R}^2) \; \forall K \in \mathcal{T}_h\} \,. \tag{5}$$

We point out that, of course, p and the directions $\boldsymbol{d}_j$ could vary between different mesh cells, and this typically occurs in practical applications of PWDG. Yet, our approach to dispersion analysis can cope only with a uniform choice of local spaces, which renders the definition (5) sufficient for our purposes.

It remains to fix the flux coefficients α and β for a complete definition of a PWDG method. In principle, any choice $\alpha, \beta > 0$ leads to a viable method, though extra restrictions may be necessary for the sake of rigorous theoretical analysis as in [10, Sect. 4], [11, Sect. 3], and [13, Sect. 4]. For the numerical experiments conducted in Section 5 we rely on the four different sets of coefficients listed in Table 1.

Here, $h > 0$ denotes the mesh width of $\mathcal{T}_h$ and, on every edge e, $c_{\mathrm{tinv}} > 0$ is minimal such that

$$\int_{\partial K} |v_h|^2 \, \mathrm{d}S \le \frac{c_{\mathrm{tinv}}^2}{\operatorname{diam} K} \int_K |v_h|^2 \, \mathrm{d}x \qquad \forall v_h \in PW_\omega(\mathbb{R}^2) \,, \tag{6}$$

for all cells $K \in \mathcal{T}_h$ containing e, cf. [10, Theorem 3.7]. The values of c_{tinv} are computed by local eigenvalue problems on $K \in \mathcal{T}_h$. The choice (UWVF) for the coefficients yields the popular UWVF discretization. The other choices (PWDG0)–(PWDG2) are inspired by numerical fluxes used for DG methods for 2nd-order elliptic problems.

3. Abstract Dispersion Analysis

We assume the triangulation $\mathcal{T}_h$ of $\Omega = \mathbb{R}^d$ to be invariant with respect to translations by the vectors $(\boldsymbol{\xi}_{\boldsymbol{n}})_{\boldsymbol{n} \in \mathbb{Z}^d}$. These vectors form a lattice in $\mathbb{R}^d$, i.e. they are the linear combinations with integer coefficients of a basis $\boldsymbol{\xi}^1, \dots, \boldsymbol{\xi}^d$.

TABLE 1. Sets of flux coefficients used for computational dispersion analysis in Section 5, cf. [10, Section 5]

	α		β
	interior	boundary	
(UWVF)	$\frac{1}{2}$	$\frac{1}{2}$	$\frac{1}{2}$
(PWDG0)	$\frac{2}{\omega h}$	$\frac{2}{\omega h}$	0
(PWDG1)	$\frac{c_{\text{tinv}}^2}{2\omega h}$	$\frac{c_{\text{tinv}}^2}{\omega h}$	0
(PWDG2)	$\frac{c_{\text{tinv}}^2}{2\omega h}$	$\frac{c_{\text{tinv}}^2}{\omega h}$	$\frac{\omega h}{10}$

Plane wave solutions $u(\boldsymbol{x}) = \exp(\mathrm{i}\omega \boldsymbol{d}\cdot\boldsymbol{x})$, $|\boldsymbol{d}| = 1$, of the Helmholtz equation are most naturally approximated by discrete Bloch waves

$$u_h(\boldsymbol{x}) = \sum_{\boldsymbol{n}\in\mathbb{Z}^d} \exp(\mathrm{i}\omega_h \boldsymbol{d}\cdot\boldsymbol{\xi_n})\widehat{u}_h(\boldsymbol{x}-\boldsymbol{\xi_n}) \tag{7}$$

where $\widehat{u}_h \in V_h$ is compactly supported, $|\boldsymbol{d}| = 1$ and $\omega_h \in \mathbb{C}$ with $\operatorname{Re}\omega_h > 0$. It is readily seen that Bloch waves are in V_h, and, although not periodic, they are characterized by

$$u_h(\boldsymbol{x}+\boldsymbol{\xi_n}) = \exp(\mathrm{i}\omega_h \boldsymbol{d}\cdot\boldsymbol{\xi_n})u_h(\boldsymbol{x}) \qquad \forall \boldsymbol{n}\in\mathbb{Z}^d\,, \tag{8}$$

thus mimicking the behaviour of the plane wave $\exp(\mathrm{i}\omega_h \boldsymbol{d}\cdot\boldsymbol{x})$.

Definition 3.1. For a prescribed direction $\boldsymbol{d}$, $|\boldsymbol{d}| = 1$, and wave number $\omega > 0$, the *discrete wave number* is the value of $\omega_h \in \mathbb{C}$ closest to ω in magnitude for which the Bloch wave (7) is a solution of the discrete equation

$$a_h(u_h, v_h) - \omega^2 (u_h, v_h)_{\mathbb{R}^d} = 0 \qquad \forall v_h \in V_h^0\,, \tag{9}$$

where V_h^0 denotes the compactly supported functions in V_h.

Dispersion in direction $\boldsymbol{d}$ manifests itself in a non-zero difference $|\omega_h - \omega|$. We can distinguish *phase dispersion* $|\operatorname{Re}\omega_h - \omega|$, which describes the error in the wavelength of the plane wave solution $\exp(\mathrm{i}\omega\boldsymbol{d}\cdot\boldsymbol{x})$, and *amplitude dispersion* or *damping* $|\operatorname{Im}\omega_h|$, which represents the change in magnitude of the discrete Bloch wave along its direction of propagation.

Remark 3.2. In PWDG methods, if the propagation direction $\boldsymbol{d}$ coincides with that of a plane wave basis function, i.e. $\boldsymbol{d} = \boldsymbol{d}_j$ in (3), then the exact solution $u(\boldsymbol{x}) = \exp(\mathrm{i}\omega\boldsymbol{d}\cdot\boldsymbol{x})$ is in V_h, and is thus recovered as the discrete solution u_h of (9). It constitutes a Bloch wave since it satisfies (8) with $\omega_h = \omega$, and consequently the dispersion in direction $\boldsymbol{d}$ is zero. This is confirmed by the numerically computed values of ω_h shown in Figure 1.

4. Numerical Computation of the Discrete Wave Number

Due to the scaling invariance of the domain $\mathbb{R}^d$, equation (9) can be rescaled to a mesh of cell size $\bar{h} = 1$; given a mesh of arbitrary cell size h, the substitution $\bar{\boldsymbol{x}} = \boldsymbol{x}/h$ transforms (9) into

$$a_{\bar{h}}(u_{\bar{h}}, v_{\bar{h}}) - \omega^2 h^2 (u_{\bar{h}}, v_{\bar{h}})_{\mathbb{R}^d} = 0 \qquad \forall v_{\bar{h}} \in V_{\bar{h}}^0\,, \tag{10}$$

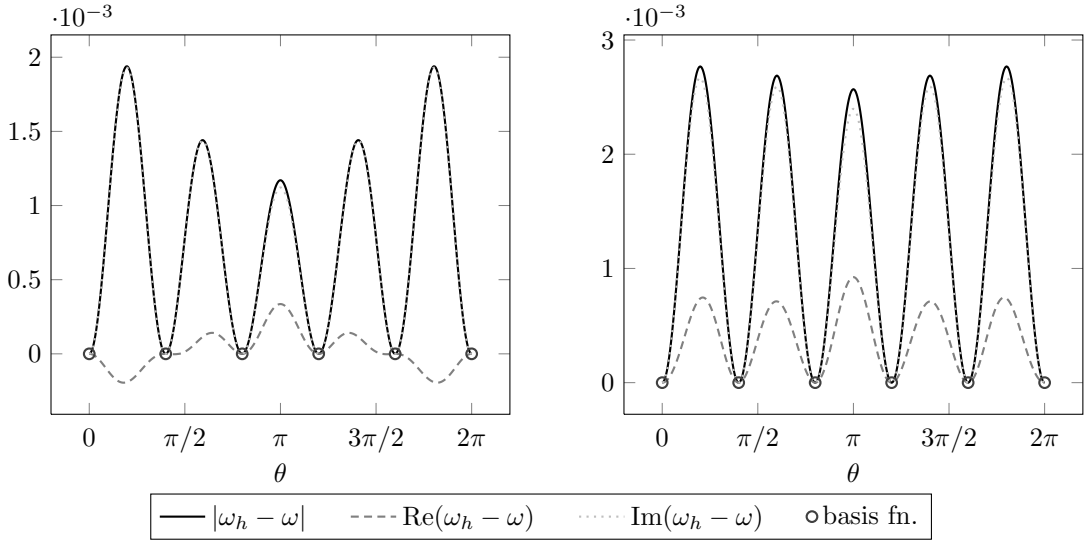

FIGURE 1. Dependence of dispersion on the direction $\boldsymbol{d} = (\cos\theta, \sin\theta)$ for (PWDG2) with $\omega = 1$ and $p = 5$ plane wave basis functions on the triangular mesh (left) and the square mesh (right) from Figure 2, computed numerically by Algorithm 4.1.

where $u_{\bar{h}}(\bar{\boldsymbol{x}}) = u_{\bar{h}}(\boldsymbol{x}/h) = u_h(\boldsymbol{x})$ and the discrete wave numbers are related by $\omega_{\bar{h}} = \omega_{\bar{h}}\bar{h} = \omega_h h$. We consequently assume, without loss of generality, that $h = 1$.

Besides the discrete wave number ω_h and the propagation direction $\boldsymbol{d}$, the remaining degrees of freedom of the discrete Bloch wave (7) are in the compactly supported function $\widehat{u}_h$. This function can be chosen in a minimal subspace $\widehat{V}_h$ of V_h that generates V_h through the translations by $(\boldsymbol{\xi_n})_{\boldsymbol{n}\in\mathbb{Z}^d}$, i.e. any $v_h \in V_h$ can be written as a sum

$$v_h(\boldsymbol{x}) = \sum_{\boldsymbol{n}\in\mathbb{Z}^d} \widehat{v}_{h,\boldsymbol{n}}(\boldsymbol{x} - \boldsymbol{\xi_n}) \,, \tag{11}$$

with $\widehat{v}_{h,\boldsymbol{n}} \in \widehat{V}_h$, and only finitely many nonzero terms in (11) at any point $\boldsymbol{x} \in \mathbb{R}^d$. For a discrete Bloch wave, $\widehat{v}_{h,\boldsymbol{n}}(\boldsymbol{x}) = \exp(\mathrm{i}\omega_h \boldsymbol{d}\cdot\boldsymbol{\xi_n})\widehat{v}_h(\boldsymbol{x})$ with $\widehat{v}_h \in \widehat{V}_h$ by (7).

In conforming Lagrangian finite elements, $\widehat{V}_h$ consists of the span of the nodal basis functions associated to a minimal set of nodes with the property that all other nodes in $\mathcal{T}_h$ are recovered through translations by $(\boldsymbol{\xi_n})_{\boldsymbol{n}\in\mathbb{Z}^d}$. In discontinuous Galerkin methods, $\widehat{V}_h$ is the restriction of V_h to a minimal patch of cells $\widehat{K} \in \mathcal{T}_h$ that generates all cells $K \in \mathcal{T}_h$ through translations by $(\boldsymbol{\xi_n})_{\boldsymbol{n}\in\mathbb{Z}^d}$. The discrete equation (9) is thus reduced from the infinite mesh $\mathcal{T}_h$ of $\mathbb{R}^d$ to a finite mesh $\widehat{\mathcal{T}}_h$, consisting just of the elements $\widehat{K}$ in a bounded domain $\widehat{\Omega}$, as illustrated in Figure 2.

Setting u_h to a Bloch wave (7) and testing with $\widehat{v}_h \in \widehat{V}_h$, (9) becomes

$$\sum_{\boldsymbol{n}\in\mathbb{Z}^d} \exp(\mathrm{i}\omega_h \boldsymbol{d}\cdot\boldsymbol{\xi_n})\big[a_h(\widehat{u}_h(\boldsymbol{x}-\boldsymbol{\xi_n}), \widehat{v}_h(\boldsymbol{x})) - \omega^2(\widehat{u}_h(\boldsymbol{x}-\boldsymbol{\xi_n}), \widehat{v}_h(\boldsymbol{x}))_{\mathbb{R}^d}\big] = 0 \qquad \forall \widehat{v}_h \in \widehat{V}_h \,, \tag{12}$$

which is a nonlinear eigenvalue problem for ω_h and $\widehat{u}_h \in \widehat{V}_h$. We point out that thanks to translation invariance of the sesquilinear forms and of the space V_h^0, testing with functions in $\widehat{V}_h$ is sufficient if u_h is a discrete Bloch wave. The sum in (12) is finite, containing only indices $\boldsymbol{n}$ for which the translated function $\widehat{u}_h(\boldsymbol{x}-\boldsymbol{\xi_n})$ interacts with $\widehat{V}_h$.

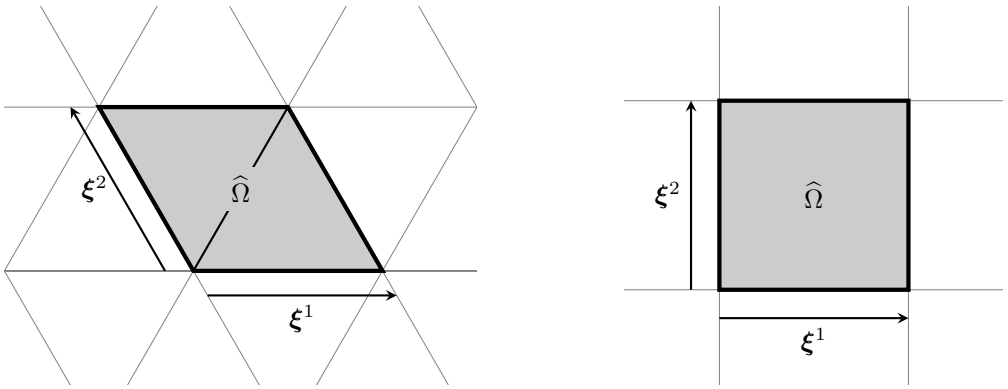

FIGURE 2. A regular triangular mesh (left) and a square mesh (right) are each generated by translations of $\widehat{\Omega}$ by the lattice $(\boldsymbol{\xi_n})_{\boldsymbol{n}\in\mathbb{Z}^2}$ with basis $\boldsymbol{\xi}^1$, $\boldsymbol{\xi}^2$, and they are invariant with respect to these translations.

To solve (12) we rely on a new fixed point iteration given by Algorithm 4.1. It reduces the nonlinear eigenvalue problem (12) for ω_h to a sequence of linear eigenvalue problems (13) for ω_k^2.

Algorithm 4.1. $\omega_0 := \omega$
For $k = 1, 2, \ldots$

- *Find* $\tilde{\omega}_k^2 \in \mathbb{C}$ *nearest to* ω^2 *and associated* $\widehat{u}_k$ *such that*

$$\tilde{\omega}_k^2 \sum_{\boldsymbol{n}\in\mathbb{Z}^d} \exp(\mathrm{i}\omega_{k-1}\boldsymbol{d}\cdot\boldsymbol{\xi_n})(\widehat{u}_k(\boldsymbol{x}-\boldsymbol{\xi_n}),\widehat{v}_h(\boldsymbol{x}))_{\mathbb{R}^d} = \sum_{\boldsymbol{n}\in\mathbb{Z}^d} \exp(\mathrm{i}\omega_{k-1}\boldsymbol{d}\cdot\boldsymbol{\xi_n}) a_h(\widehat{u}_k(\boldsymbol{x}-\boldsymbol{\xi_n}),\widehat{v}_h(\boldsymbol{x})) \qquad \forall \widehat{v}_h \in \widehat{V}_h\ . \quad (13)$$

- *Update* $\omega_k := \omega_{k-1} + \omega - \tilde{\omega}_k$.

Theorem 4.2. *If the sequence* $(\omega_k)_{k=0}^{\infty}$ *converges, its limit is a solution* ω_h *of* (12).

Proof. Let ω_∞ denote the limit of $(\omega_k)_{k=0}^{\infty}$. Since $\omega - \tilde{\omega}_k = \omega_k - \omega_{k-1}$, convergence of $(\omega_k)_{k=0}^{\infty}$ implies $\tilde{\omega}_k \to \omega$.

Let (13) be cast as a matrix eigenvalue problem $A(\omega_{k-1})\boldsymbol{u}_k = \tilde{\omega}_k^2 \boldsymbol{u}_k$, where the matrix $A(\omega_{k-1})$ depends continuously on ω_{k-1} and $\boldsymbol{u}_k$ is a suitable vector representation of $\widehat{u}_k$. The assumed convergence $\omega_k \to \omega_\infty$ implies that the matrices $A(\omega_{k-1})$ converge in norm to $A(\omega_\infty)$. Since $\tilde{\omega}_k^2$ is an eigenvalue of $A(\omega_{k-1})$, its limit ω^2 is an eigenvalue of $A(\omega_\infty)$. Consequently, for the function $\widehat{u}_\infty \in \widehat{V}_h$ represented by the corresponding eigenvector,

$$\tilde{\omega}^2 \sum_{\boldsymbol{n}\in\mathbb{Z}^d} \exp(\mathrm{i}\omega_\infty\boldsymbol{d}\cdot\boldsymbol{\xi_n})(\widehat{u}_\infty(\boldsymbol{x}-\boldsymbol{\xi_n}),\widehat{v}_h(\boldsymbol{x}))_{\mathbb{R}^d} = \sum_{\boldsymbol{n}\in\mathbb{Z}^d} \exp(\mathrm{i}\omega_\infty\boldsymbol{d}\cdot\boldsymbol{\xi_n}) a_h(\widehat{u}_\infty(\boldsymbol{x}-\boldsymbol{\xi_n}),\widehat{v}_h(\boldsymbol{x})) \qquad \forall \widehat{v}_h \in \widehat{V}_h\ , \quad (14)$$

which is equivalent to (12) with $\omega_h = \omega_\infty$. □

Invariably, we observed fast linear convergence for Algorithm 4.1, as illustrated in Figure 3 for a particular case. Taking this for granted, the total error $|\omega_k - \omega_h|$ is bounded by a small multiple of the size of the increment $|\omega_k - \omega_{k+1}|$. Thus, we terminate the iteration, when the size of the increment $\omega_k - \omega_{k-1} = \omega - \tilde{\omega}_k$ drops below a prescribed relative (w.r.t. $|\omega|$) tolerance.

Remark 4.3. For discontinuous Galerkin methods with sesquilinear forms (2), interactions between cells are limited to cells sharing an edge ($d = 2$) or face ($d = 3$), and thus the sum in (12) can be restricted to $\{-1, 0, 1\}^d$, or a subset, depending on the symmetry of $\mathcal{T}_h$. This carries over to (13), and since degrees of freedom on

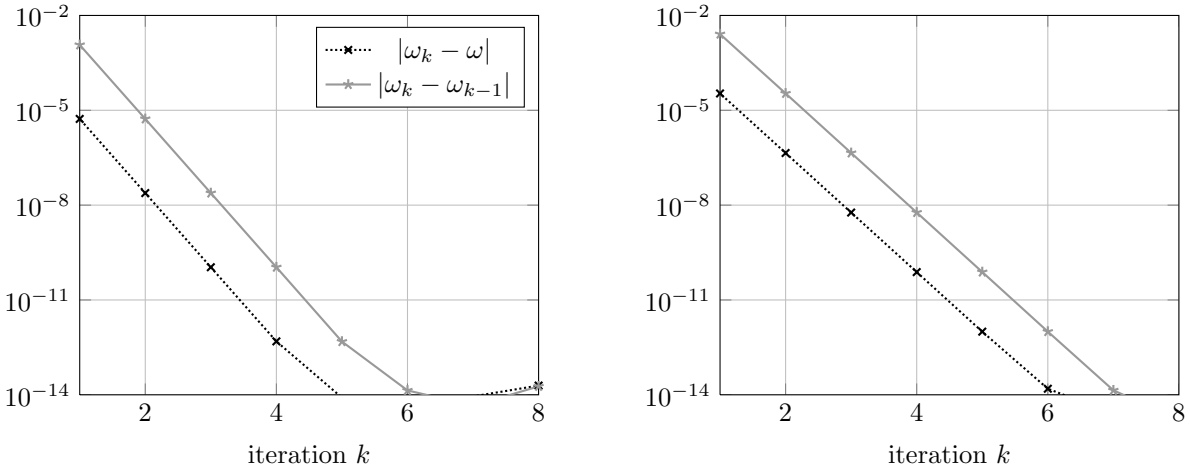

FIGURE 3. Convergence of Algorithm 4.1 on the regular triangular mesh (left) and the square mesh (right) for $\omega = 1$ with $p = 5$ equispaced plane wave basis functions, for measuring dispersion in the direction $\boldsymbol{d} = (-1, 0)$, i.e. for $\theta = \pi$.

different cells have mutually disjoint supports, (13) simplifies to

$$\tilde{\omega}_k^2(\widehat{u}_k(\boldsymbol{x}), \widehat{v}_h(\boldsymbol{x}))_{\mathbb{R}^d} = \sum_{\boldsymbol{n}\in\{-1,0,1\}^d} \exp(\mathrm{i}\omega_{k-1}\boldsymbol{d}\cdot\boldsymbol{\xi_n}) a_h(\widehat{u}_k(\boldsymbol{x}-\boldsymbol{\xi_n}), \widehat{v}_h(\boldsymbol{x})) \qquad \forall \widehat{v}_h \in \widehat{V}_h \,. \tag{15}$$

5. Dispersion of PWDG: Numerical Computations

Consistency of Galerkin methods entails that the use of plane wave basis functions eliminates dispersion in the propagation directions of the basis functions, as noted in Remark 3.2 and illustrated in Figure 1. Figure 4 adds the dependence on the rotation ψ in the definition (4) of the plane wave basis functions. Evidently, the directions in which dispersion vanishes track the propagation directions of the plane wave basis functions as these are rotated. Furthermore, Figure 5 indicates that dispersion decays in all directions as ω is decreased.

These computations and all of the following use the triangular and square meshes depicted in Figure 2. The mesh width h, denoting the lengths of all edges in these meshes, is scaled to $h = 1$. All numerical values of dispersion are approximations computed by Algorithm 4.1, which is terminated when $|\tilde{\omega}_k - \omega| \leq 10^{-3}\omega$. The values of c_{tinv} from (6) are set to $c_{\mathrm{tinv}} = 4.6568$ on the triangular mesh and $c_{\mathrm{tinv}} = 4.1040$ on the square mesh.

We study the maximal dispersion for a given number of plane wave basis functions by taking the maximum over a large number of equidistant (in angle) directions $\boldsymbol{d} = (\cos\theta, \sin\theta)$ and ten separate values of ψ in (4) to account for the relative orientation of the propagation directions of the basis functions as compared to the mesh. In order to improve the initial guess in Algorithm 4.1, we begin these computations at directions equal to propagation directions of basis functions, and incrementally move away from these, using each value of ω_h as the initial guess for the discrete wave number in the next direction.

Figure 6 shows the dependence of the maximal dispersion on ω for $p = 5$ and the four sets of flux parameters listed in Table 1. For all four, dispersion decreases algebraically as $\omega \to 0$. The rate of decay seems to coincide for (PWDG0)–(PWDG2), but is slower for (UWVF). This disparity is no longer evident when considering only the phase dispersion as in Figure 7, suggesting that the extra dispersion of (UWVF) is due only to damping. For large ω when the plane waves can no longer be resolved by V_h, multiple solutions ω_h of (12) are comparably close to ω, rendering the problem of determining the dispersion ill-posed.

In order to quantify the decay rate of the dispersion as $\omega \to 0$, we approximate curves such as those in Figure 6 by lines in bilogarithmic scale by means of weighted least squares with weight ω^{-2}. This suggests a

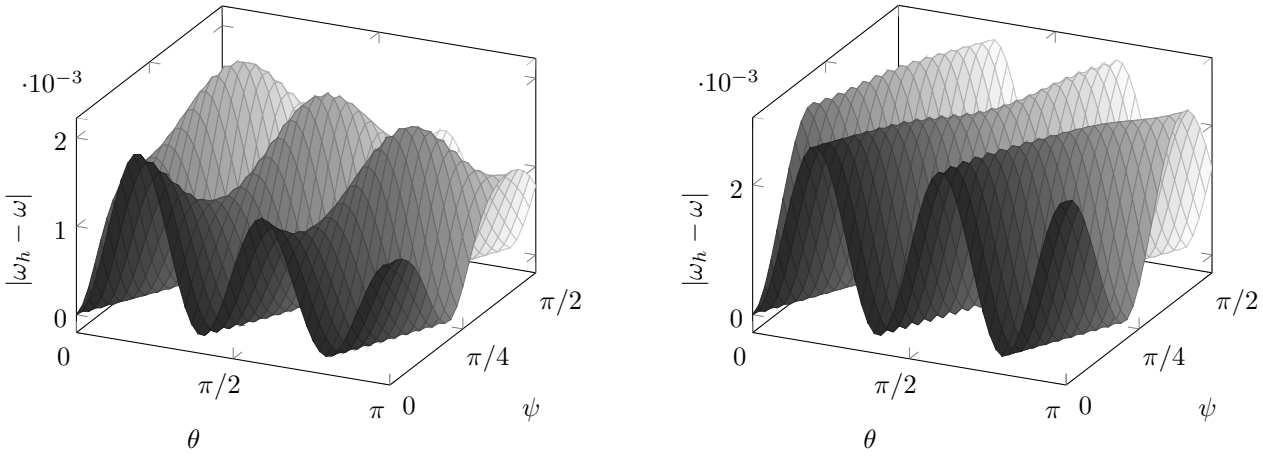

FIGURE 4. Dependence of the dispersion of (PWDG2) on the direction $\boldsymbol{d} = (\cos\theta, \sin\theta)$ and the rotation ψ in the definition (4) of the plane wave basis functions for $p = 5$ and $\omega = 1$ on a triangular mesh (left) and a square mesh (right).

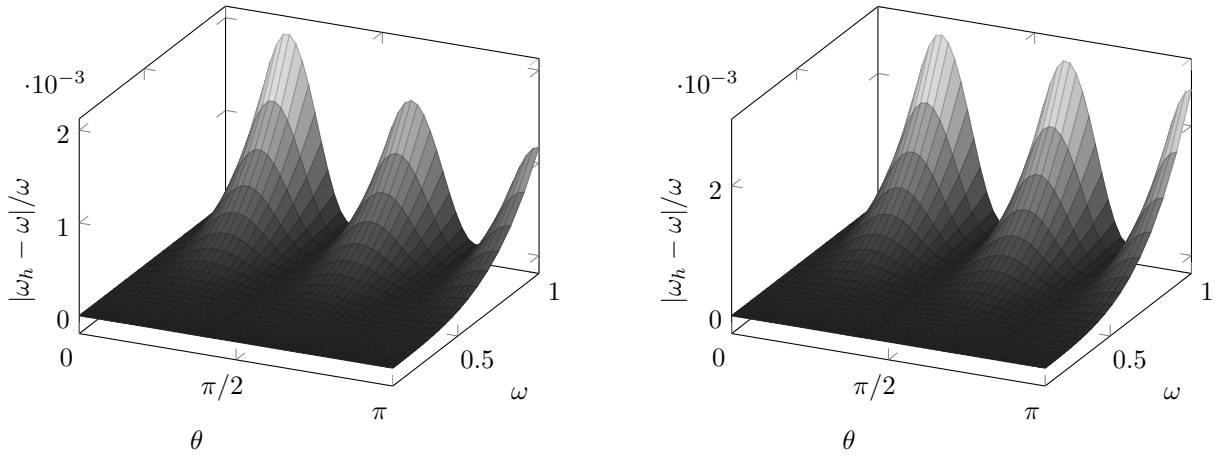

FIGURE 5. Dependence of the dispersion of (PWDG2) on the direction $\boldsymbol{d} = (\cos\theta, \sin\theta)$ and ω for $p = 5$ plane wave basis functions on a triangular mesh (left) and a square mesh (right).

behavior of the maximal dispersion according to

$$\max \frac{1}{\omega}|\omega_h - \omega| \approx c\omega^{\eta} \quad \text{for } \omega \to 0. \tag{16}$$

Numerically determined values of η and c depending on p are plotted in Figures 8 and 9. For the fluxes (PWDG0)–(PWDG2), these computations suggest

$$\eta = 2\left\lfloor \frac{p-1}{2} \right\rfloor, \tag{17}$$

while η is further reduced by one for (UWVF), except for $p = 3, 4$ in the case of a triangular mesh. This even/odd staircase effect also appears in the approximation properties of plane waves in two dimensions, see [10].

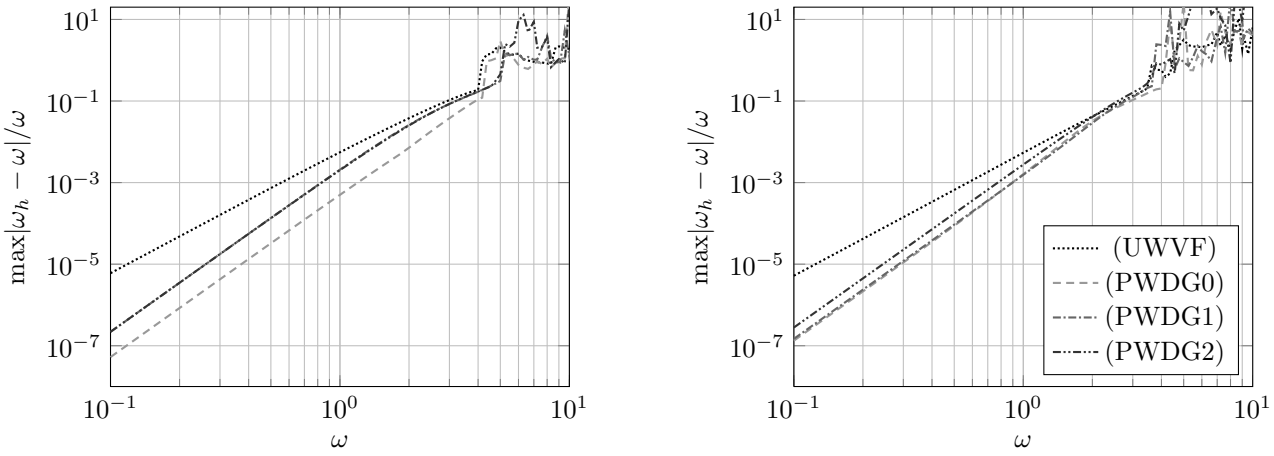

FIGURE 6. Dependence of the dispersion on ω for the fluxes listed in Table 1 on a triangular mesh (left) and a square mesh (right), using $p = 5$ local plane wave basis functions.

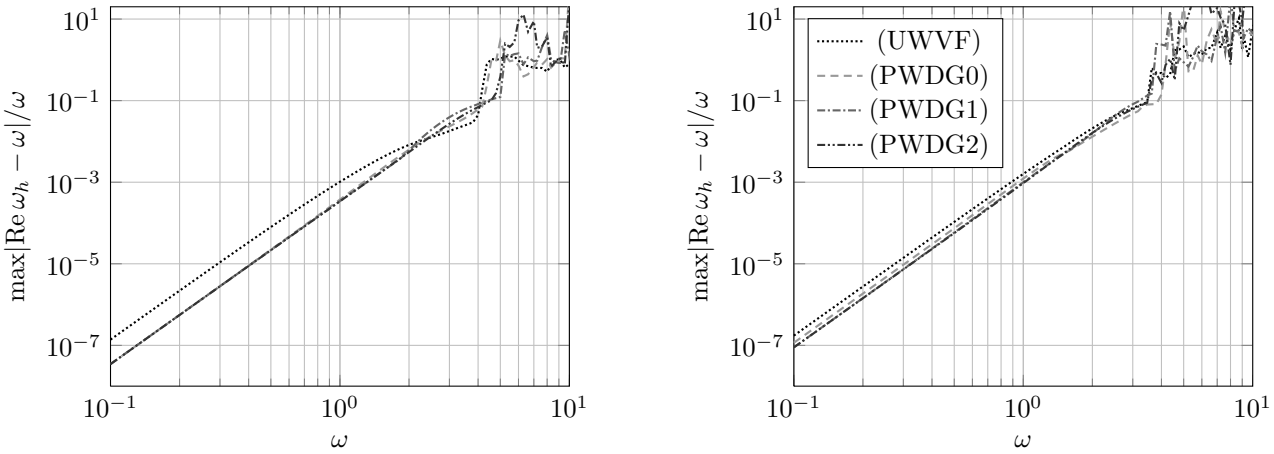

FIGURE 7. Dependence of the phase dispersion on ω for the fluxes listed in Table 1 on a triangular mesh (left) and a square mesh (right), using $p = 5$ local plane wave basis functions.

Figure 9 reveals an exponential decay of the maximal dispersion for small ω as p is increased. This is confirmed and extended to larger ω by the data from Figures 10 and 11, which plot the maximal dispersion for large p and ω. The erratic behavior of the dispersion for small ω can be blamed on numerical instabilities due to the near linear dependence of plane wave basis functions.

Finally, the dispersion of PWDG methods is compared to that of conforming finite elements with tensor product polynomial bases on the square mesh of $\mathbb{R}^2$ for $\omega = 4$ in Figure 12. When considered as a function of the effective polynomial degree, the dispersion of PWDG methods is slightly larger than that of FEM. However, since the dimension of the local approximation space $\widehat{V}_h$ scales quadratically in the polynomial degree for FEM, but only linearly in the number of plane wave basis functions for PWDG, the dispersion of PWDG methods decreases much faster than that of FEM when considered as a function of $\dim \widehat{V}_h$.

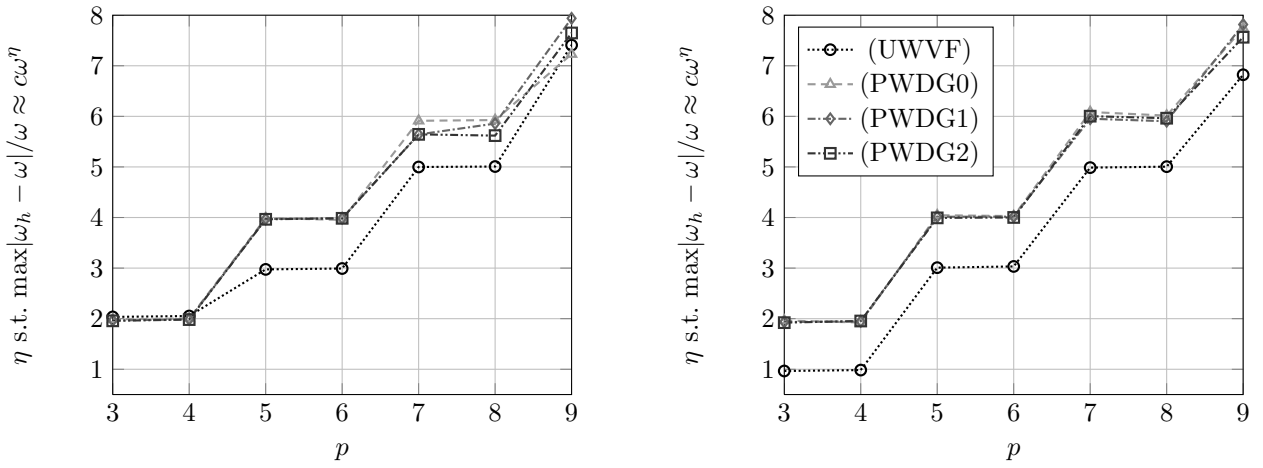

FIGURE 8. Numerically determined values of η in (16) for a triangular mesh (left) and a square mesh (right).

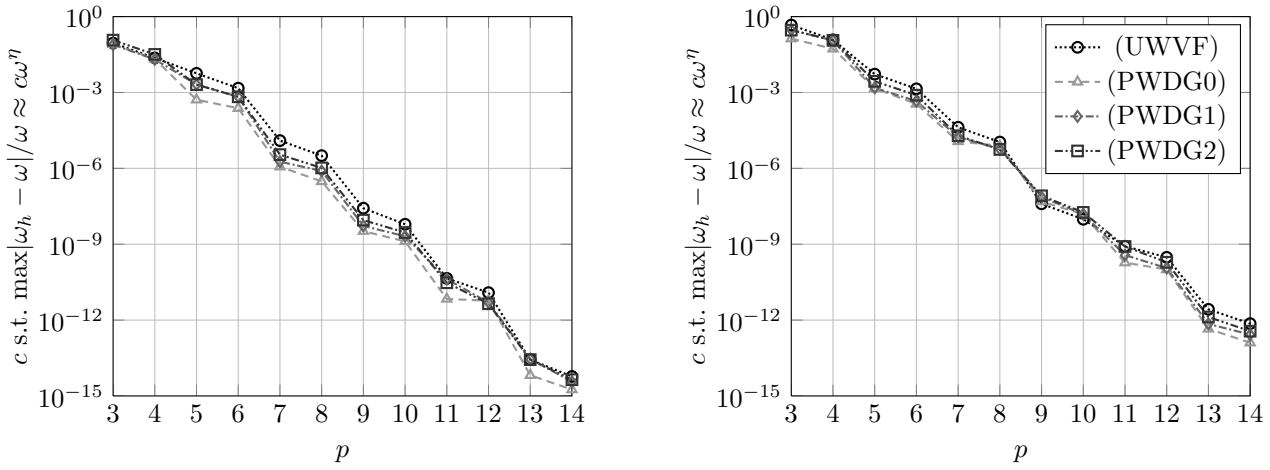

FIGURE 9. Numerically determined values of c in (16) for a triangular mesh (left) and a square mesh (right).

REFERENCES

[1] AINSWORTH, M. Discrete dispersion relation for hp-version finite element approximation at high wave number. *SIAM J. Numer. Anal. 42*, 2 (2004), 563–575.

[2] AINSWORTH, M. Discrete dispersion relation for *hp*-version finite element approximation at high wave number. *SIAM J. Numer. Anal. 42*, 2 (2004), 553–575 (electronic).

[3] AINSWORTH, M. Dispersive and dissipative behaviour of high order discontinuous Galerkin finite element methods. *J. Comp. Phys. 198*, 1 (2004), 106–130.

[4] AINSWORTH, M. Dispersive properties of high order Nedelec/edge element approximation of the time-harmonic Maxwell equations. *Phil. Trans. Roy. Soc. Series A 362*, 1816 (2004), 471–493.

[5] AINSWORTH, M., MONK, P., AND MUNIZ, W. Dispersive and dissipative properties of discontinuous Galerkin finite element methods for the second-order wave equation. *J. Sci. Comput. 27*, 1-3 (2006), 5–40.

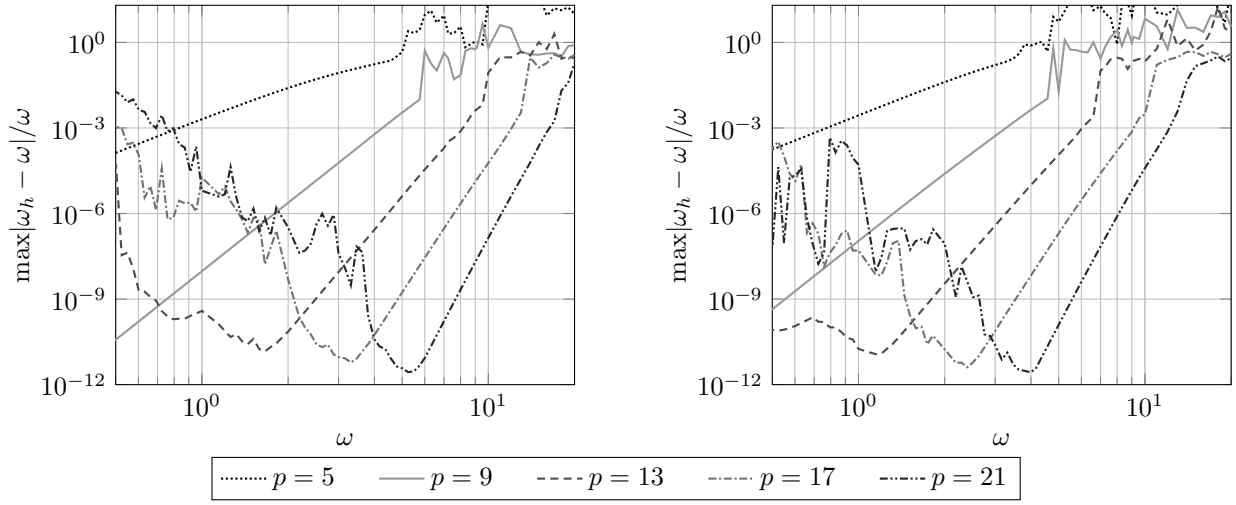

FIGURE 10. Dependence of the dispersion of (PWDG2) on ω for various p on a triangular mesh (left) and a square mesh (right). Numerical instability of Algorithm 4.1 sets in for small ω and large p.

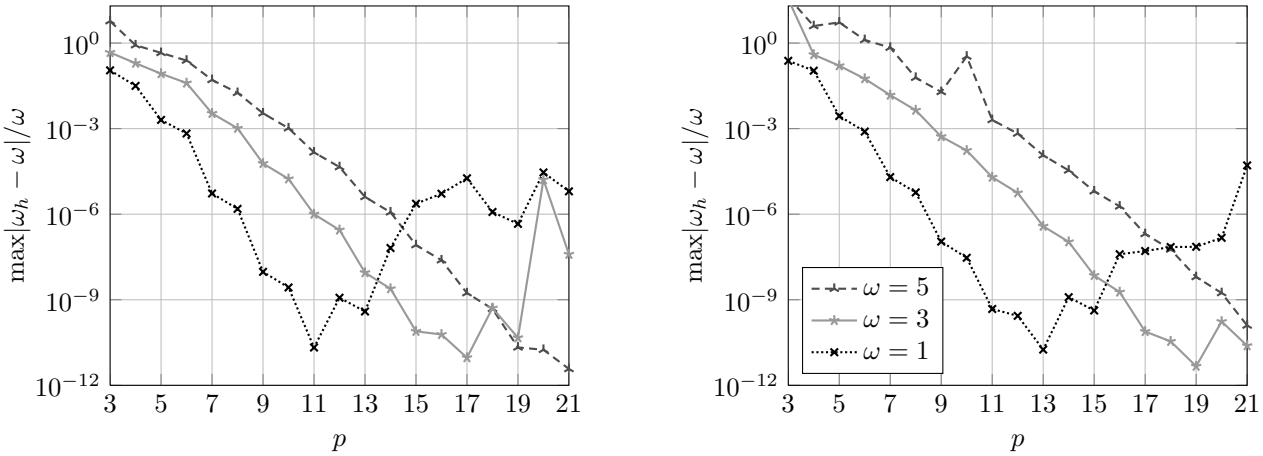

FIGURE 11. Dependence of the dispersion of (PWDG2) on p for $\omega \in \{1, 3, 5\}$ on a triangular mesh (left) and a square mesh (right).

[6] BABUŠKA, I., AND SAUTER, S. Is the pollution effect of the FEM avoidable for the Helmholtz equation? *SIAM Review 42*, 3 (September 2000), 451–484.

[7] CESSENAT, O., AND DESPRÉS, B. Application of an ultra weak variational formulation of elliptic PDEs to the two-dimensional Helmholtz equation. *SIAM J. Numer. Anal. 35*, 1 (1998), 255–299.

[8] CESSENAT, O., AND DESPRÉS, B. Using plane waves as base functions for solving time harmonic equations with the ultra weak variational formulation. *J. Computational Acoustics 11* (2003), 227–238.

[9] DERAEMAEKER, A., BABUŠKA, I., AND BOUILLARD, P. Dispersion and pollution of the FEM solution for the Helmholtz equation in one, two, and three dimensions. *Int. J. Numer. Meth. Engr. 46* (1999), 471–499.

[10] GITTELSON, C., HIPTMAIR, R., AND PERUGIA, I. Plane wave discontinuous Galerkin methods: Analysis of the h-version. *Math. Model. Numer. Anal. 43* (2009), 297–331.

[11] HIPTMAIR, R., MOIOLA, A., AND PERUGIA, I. Plane wave discontinuous Galerkin methods for the 2d Helmholtz equation: Analysis of the p-version. *SIAM J. Numer. Anal. 49*, 1 (2011), 264–284.

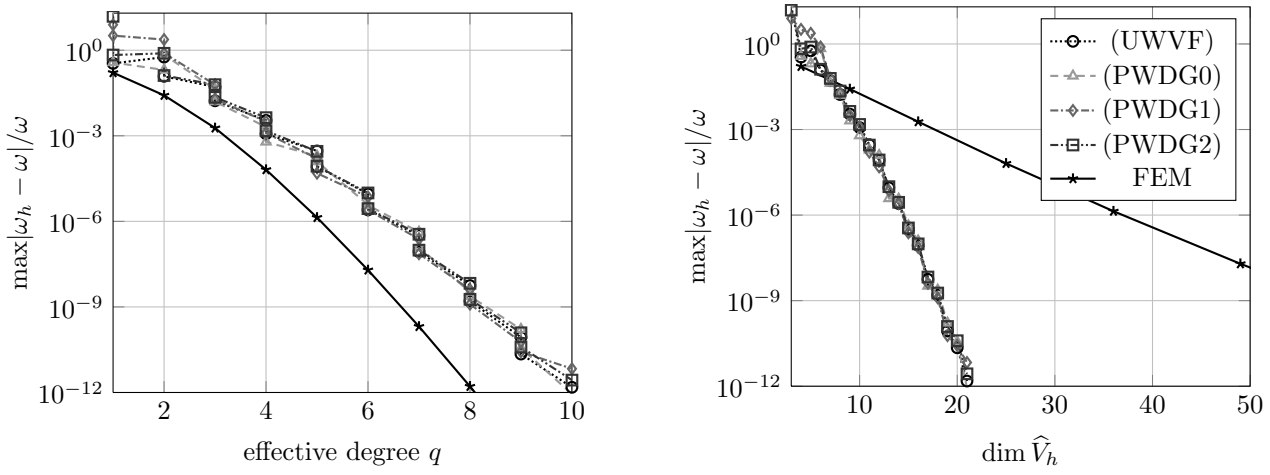

FIGURE 12. Comparison of the dispersion of PWDG methods with tensor product Lagrangian finite elements on a square mesh with $\omega = 4$. For PWDG with p plane wave basis functions, the local dimension is $\dim \widehat{V}_h = p$ and the effective polynomial degree is $q = \lfloor (p-1)/2 \rfloor$. For FEM with polynomial degree q, the local dimension is $\dim \widehat{V}_h = (q+1)^2$. Discrete wave numbers for FEM are computed by the explicit formula in [2].

[12] HIPTMAIR, R., MOIOLA, A., AND PERUGIA, I. Stability results for the time-harmonic maxwell equations with impedance boundary conditions. *Math. Model Meth. Appl. Sci. 21*, 11 (2011), 2263–2287.

[13] HIPTMAIR, R., MOIOLA, A., AND PERUGIA, I. Trefftz discontinuous Galerkin methods for acoustic scattering on locally refined meshes. Report 2012-06, SAM, ETH Zürich, Zürich, Switzerland, 2012. submitted to APNUM.

[14] HUTTUNEN, T., MALINEN, M., AND MONK, P. Solving Maxwell's equations using the ultra weak variational formulation. *J. Comp. Phys. 223* (2007), 731–758.

[15] HUTTUNEN, T., MONK, P., AND KAIPIO, J. Computational aspects of the ultra-weak variational formulation. *J. Comp. Phys. 182*, 1 (2002), 27–46.

[16] IHLENBURG, F., AND BABUŠKA, I. Finite element solution of the Helmholtz equation with high wave number. Part I: The h-version of the FEM. *Computers Math. Appl. 30*, 6 (1995), 9–37.

[17] TUNCER, O., NAIR, N., SHANKER, B., AND KEMPEL, L. Dispersion analysis in scalar generalized finite element method. In *Antennas and Propagation Society International Symposium, 2008. AP-S 2008. IEEE* (july 2008), pp. 1 –4.

Recent Research Reports

Nr.	Authors/Title

2012-32 A. Lang and S. Larsson and C. Schwab
Covariance structure of parabolic stochastic partial differential equations

2012-33 R. Hiptmair and C. Jerez-Hanckes and S. Mao
Extension by zero in discrete trace spaces: Inverse estimates

2012-34 R. Hiptmair and C. Schwab and C. Jerez-Hanckes
Sparse tensor edge elements

2012-35 S. Mishra and N. H. Risebro and C. Schwab and S. Tokareva
Numerical solution of scalar conservation laws with random flux functions

2012-36 R. Hiptmair and L. Kielhorn
BETL — A generic boundary element template library

2012-37 C. Schillings and C. Schwab
Sparse, adaptive Smolyak algorithms for Bayesian inverse problems

2012-38 R. Hiptmair and A. Moiola and I. Perugia and C. Schwab
Approximation by harmonic polynomials in star-shaped domains and exponential convergence of Trefftz hp-DGFEM

2012-39 A. Buffa and G. Sangalli and Ch. Schwab
Exponential convergence of the hp version of isogeometric analysis in 1D

2012-40 D. Schoetzau and C. Schwab and T. Wihler and M. Wirz
Exponential convergence of hp-DGFEM for elliptic problems in polyhedral domains

2012-41 M. Hansen
n-term approximation rates and Besov regularity for elliptic PDEs on polyhedral domains